Reprinted from

Medical Physics

May/June 1985 Volume 12, Number 3

A large-angle coherent/Compton scattering method for measurement *in vitro* of trabecular bone mineral concentration

G. E. Gigante
Dipartimento di Scienze Biomediche dell'Universita' dell'Aquila, l'Aquila, Italy 67100

S. Sciuti
Dipartimento di Energetica e Centro per l'Ingegneria Biomedica dell'Universita di Roma "La Sapienza," Corso Vittoria Emmanuele II, 244, Roma, Italy 00186

pp. 321-326

Published for the
American Association of Physicists in Medicine
by the American Institute of Physics

A large-angle coherent/Compton scattering method for measurement *in vitro* of trabecular bone mineral concentration

G. E. Gigante
Dipartimento di Scienze Biomediche dell'Universita' dell'Aquila, l'Aquila, Italy 67100

S. Sciuti
Dipartimento di Energetica e Centro per l'Ingegneria Biomedica dell'Universita di Roma "La Sapienza," Corso Vittorio Emmanuele II, 244, Roma, Italy 00186

(Received 2 May 1984; accepted for publication 17 October 1984)

In this paper, experiments and related theoretical deductions on coherent/Compton scattering of 59.5-keV Am^{241} gamma line by bonelike materials are described. In particular, we demonstrate that a photon scattering mineralometer (PSM) can attain the best working conditions when it operates in a backscattering geometry mode. In fact, the large scattering angle we chose, $\vartheta = 135°$, allowed us to assemble a very compact source–detector device. Further, the relative sensitivity at 135° turns out to be $\simeq$1.7 and $\simeq$6 times bigger than at 90° and 45°, respectively. The performances of the $\vartheta = 135°$ PSM we assembled were experimentally investigated; i.e., in a measuring time of 10^3 s, a $\simeq 5‰$ statistical precision for bonelike materials, such as K_2HPO_4–water solutions, was obtained. The large-angle PSM device seems therefore to be very promising for trabecular bone mineral density measurements *in vivo* in peripheral anatomic sites.

I. INTRODUCTION

Accurate measurements of bone mineral content (BMC) *in vivo* are requested for many diagnostic purposes. In order to evaluate the bone mineral weight fraction, which is related to the trabecular bone mineral density (TBMD), the ratio $R = I_r/I_c$ can be measured, where I_r and I_c are, respectively, the elastic Rayleigh, and inelastic Compton, scattered intensities.[1–6] The R ratio turns out to be very sensitive to TBMD through the physical parameter Z_{eff}, i.e., the bone tissue effective atomic number.[4,7] TBMD measurements *in vitro* can be performed with an accuracy within a few percent, requiring counting times in the order of 10^2–10^3 s.[2,3] Therefore the applications *in vivo* could be very promising when related to particular bone sites.

The fact that the R ratio falls, as $\vartheta^{-2,3}$, due to the rapid decrease of the elastic intensity with scattering angle, has led many authors to operate at small ($\vartheta < 90°$) scattering angles. Low scattering angle geometry, however, can give rise to some disadvantages, such as an increase of instrumental error, due to partial overlapping of scattering peak areas and to direct radiation background. Moreover, some troubles arising from the scattering volume shape can occur.[3]

Kerr *et al.*[2] have shown that, in coherent scattering experiments, the more appropriate excitation energy falls in the range of 60–80 keV, as a compromise between the coherent scattering cross section, the self-absorption effect, and the detector efficiency.

Further, Leichter *et al.*[5] pointed out that relative sensitivity must be taken into account in order to find optimal γ-ray energy.

Karellas *et al.*,[4] operating in the scattering angle range $30° < \vartheta < 98°$ stated that TBMD sensitivity *in vitro* increases with the scattering angle.

In the present work, a large-angle ($\vartheta = 135°$) photon scattering mineralometer (PSM) is described. The device operates with 59.5-keV γ line, and is characterized by a very compact source–detector measuring head. The relative sensitivity, precision, and related results are given. Further, the statistical error and accuracy in dealing with a backscattering geometry are discussed.

II. THEORY

Referring to Fig. 1, let us consider a well-collimated photon beam of energy E_0, intersecting the detector axis at a point inside a piece of matter of atomic number Z and density d. Then we can write for the R ratio at scattering angle ϑ:

$$R = \frac{d\sigma_T/d\Omega}{d\sigma_{KN}/d\Omega}\,\frac{F_z^2(E_0,\vartheta)}{S_z(E_0,\vartheta)} = \frac{(\mu/d)_{R,Z}}{(\mu/d)_{C,z}}, \tag{1}$$

where $d\sigma_T/d\Omega$ = differential Thomson cross section, $d\sigma_{KN}/d\Omega$ = Klein–Nishina differential cross section, $F_z(E_0,\vartheta)$ = atomic form factor for coherent scattering,[8] $S_z(E_0,\vartheta)$ = incoherent scattering function,[8] A = atomic weight, $(\mu/d)_{R,Z} = (d\sigma_T/d\Omega)\times(F_z^2/A)$, and $(\mu/d)_{C,z} = (d\sigma_{KN}/d\Omega)\times(S_z/A)$.

For a multielemental target we can write

$$R = \frac{\Sigma(\mu/d)_{R,i}\,W_i}{\Sigma(\mu/d)_{C,i}\,W_i}\,G, \tag{2}$$

where the W's are the weight fractions and G is a correcting function dealing with absorption and self-absorption effects of interposed tissues. As is well known,[2,4,5] Eq. (2) shows that the sensitivity depends mainly on E_0 and ϑ. Furthermore,

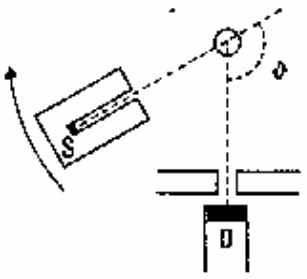

FIG. 1. Sketch of the variable angle scattering device for angular dependence evaluations; S = source, D = detector.

 0094-2405/85/030321-06$01.20

the R ratio allows one to disregard some important parameters, such as efficiencies, primary photon intensity, and density.

As far as low-Z materials are concerned, the primary photon energy E_0 can be fixed at 60 keV.[2,4]

In Fig. 2, curves of R versus Z in the range $6<Z<20$ at three different scattering angles are reported. The ln–ln approximation in the same Z range gives the following results:

$$R = A(E_0, \vartheta)Z^n, \tag{3}$$

where $n = 1.4$ for $\vartheta = 45°$, 3.2 for $\vartheta = 90°$, and 4.2 for $\vartheta = 135°$.

These results clearly show that, for $Z<20$, the relative variation $(dR/dZ)/R$ improves, increasing the scattering angle.

Further, the following simplified relation:

$$R = \Sigma_i W_i R_i \tag{4}$$

allows one to calculate the R ratio for any compound of Z_1, Z_2, ... elements, with a good approximation.[7]

By combining Eqs. (3) and (4), we can introduce an effective atomic number for a given compound,

$$Z_{\text{eff}} = (\Sigma_i W_i Z_i^n)^{1/n}. \tag{5}$$

From Eqs. (3) and (5), it follows that Z_{eff} increases with the scattering angle.

A useful simplification of Eq. (2) applies when the sample to be analyzed can be represented by a binary mixture, as occurs for soft tissue (st) and bone mineral (bm) in the trabecular bone. In these cases we can write

$$R = \frac{(\mu/d)_{R,\text{bm}} W_{\text{bm}} + (\mu/d)_{R,\text{st}} W_{\text{st}}}{(\mu/d)_{C,\text{bm}} W_{\text{bm}} + (\mu/d)_{C,\text{st}} W_{\text{st}}} G$$

$$\simeq (R_{\text{bm}} W_{\text{bm}} + R_{\text{st}} W_{\text{st}})G. \tag{6}$$

The linear approximation in Eq. (6) holds because $(\mu/d)_{C,\text{bm}} \simeq (\mu/d)_{C,\text{st}}$.

According to Eq. (6), the sensitivity can be written, taking $G = 1$, as

$$dR/dW_{\text{bm}} = R_{\text{bm}} - R_{\text{st}}. \tag{7}$$

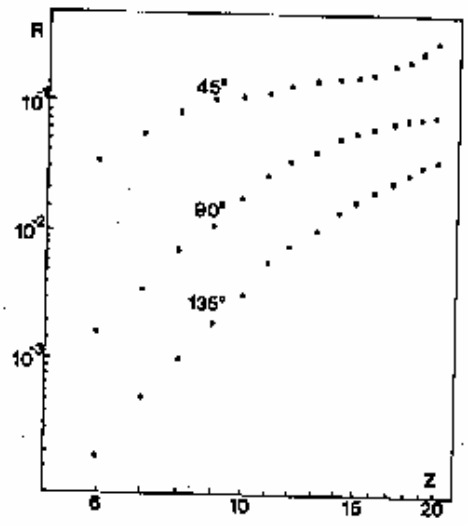

FIG. 2. ln–ln plot of the calculated coherent/Compton ratio R vs atomic number Z at three different scattering angles.

From Eqs. (3), (5), and (7), it turns out that the relative sensitivity $(dR/dW_{\text{bm}})/R$ increases with the scattering angle (see Sec. IV A).

Finally, the calculated statistical error in the measurements of W_{bm} in a 1σ approximation can be written as

$$\Delta W_{\text{bm}} = \frac{\sigma(R)}{R_{\text{bm}} - R_{\text{st}}} = \frac{1}{\sqrt{I_\gamma}} \frac{R}{(R_{\text{bm}} - R_{\text{st}})}, \tag{8}$$

where $\sigma(R) \simeq R/\sqrt{I_\gamma}$.

Equation (8) shows that, for a given I_γ, ΔW_{bm} improves with ϑ, due to the relative sensitivity increase.

III. MATERIALS AND METHODS

Two different experimental devices were employed. The first one is a variable angle spectrometer, schematically depicted in Fig. 1. A 7.4-GBq (200 mCi) Am^{241} point source, housed in a suitable lead collimator, was mounted on a rotating table of an x-ray spectrometer. An x-ray hyperpure Ge detector and multichannel analyzer completed the device. Cylindrical boxes (32-mm diameter × 35-mm height) containing $Ca_3(PO_4)_2$ suspensions in glycerine were used as bonelike material.

The working conditions were kept constant at different scattering angles (measuring time = 400 s), while the Compton-peak integration limits were changed for each angle at a constant channel interval.

The second device is the *ad hoc* designed mineralometer, referred to as PSM, operating at a fixed large angle $\vartheta = 135°$. The PSM device, expressly developed for feasibility studies on peripheral trabecular bone sites, is schematically depicted in Fig. 3. Two 1.67-GBq (45 mCi) Am^{241} point sources, a hyperpure Ge x-ray detector, an analogic electronic chain, and a microprocessor were employed. Sources and detector are assembled to form a compact unit, the measuring head, which can be moved along the counter axis according to displacements as small as 1 mm.

The PSM was calibrated by using K_2HPO_4–water solutions in the 0%–60% concentration range, in 20-mm-thick containers. In Fig. 4, a typical spectrum, as observed with the PSM device, is shown.

The interposed soft-tissue effects were simulated with a 5-mm-thick Plexiglas sheet.

A cadmium strip was used in order to verify the scattering volume (SV) profile along the h axis.

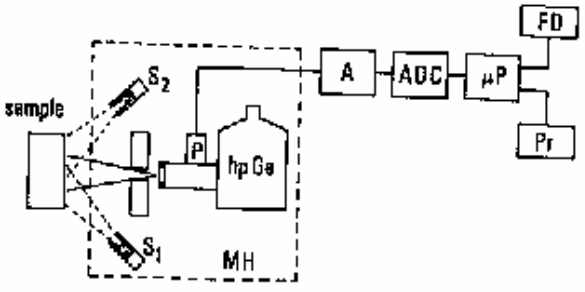

FIG. 3. Schematic representation of the $\vartheta = 135°$ photon scattering mineralometer (PSM): S_1 and S_2 are Am^{241} point sources, hpGe = hyperpure Ge detector; MH = measuring head, μP = microcomputer, FD = floppy disk, Pr = printer.

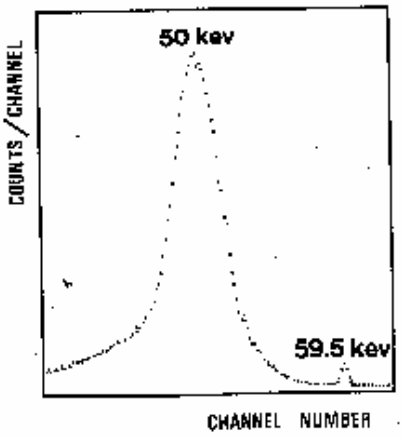

FIG. 4. The spectrum of scattered 59.5-keV Am^{241} γ rays at $\vartheta = 135°$, as recorded by the PSM described in the text.

In order to measure the response function R vs SV thickness, a cylindrical container provided with a movable piston and filled with a 40% K_2HPO_4–water solution was used. The SV thickness was varied by means of the movable piston. The background correction concerning the coherent peak has been evaluated by using a straight line approximation.

All of the measurements carried out with the PSM lasted 1000 s.

IV. RESULTS

A. Angular dependence of the response function

The variable angle device was primarily used to find the best working conditions required for designing the second device, i.e., the bone-dedicated PSM. To this aim, the relative sensitivity versus scattering angle was measured for glycerine–$Ca_3(PO_4)_2$ mixtures. In Fig. 5, the experimental behavior of R versus W is given in a ln–ln representation at three different angles.

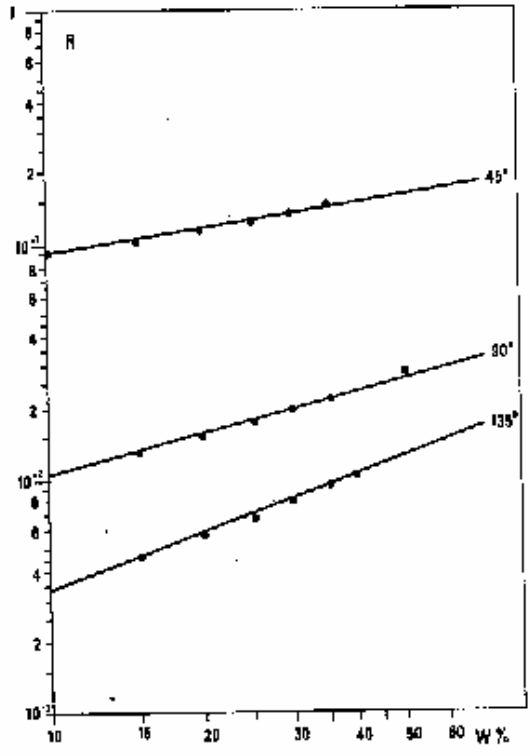

FIG. 5. ln–ln plots of experimental coherent/Compton ratio R vs $Ca_3(PO_4)_2$ concentration in glycerine solutions, at three different angles.

TABLE I. Measured and calculated sensitivities S, and measured and calculated relative sensitivities (S/R_{gly}), deduced from least-mean-squares fits.

Scattering angle	$S = dR/dW$ Theoretical	Experimental	S/R_{gly} Theoretical	Experimental[a]
45°	0.12	0.17	2.1	1.9
90°	0.04	0.044	9.3	5.8
135°	0.017	0.022	27	10

[a] Without background subtraction on coherent peak area.

The measured sensitivities S, as deduced from least-mean-squares fits, are reported in Table I, together with the calculated ones.

The measured and calculated relative sensitivities (S/R_{gly}), taking glycerine (R_{gly}) as reference, are also reported.

It is to be noted that the statistical error, Eq. (8), does not significantly improve by increasing ϑ because the coherent scattering counting rate strongly decreases. For example, operating at constant counting time (400 s), the measured statistical errors deduced for a 30% $Ca_3(PO_4)_2$ mixture are 1.2% at 45°, 1.1% at 90°, and 1.1% at 135°.

The above stated results showed the opportunity of operating at large scattering angles, i.e., $\vartheta = 135°$, provided that a compact source–detector assembly is employed which is characterized by (1) small overall dimensions, so that it can easily be pointed in any desired direction and it can get near to any part of a sample; (2) very short source–sample and sample–detector lengths, in order to obtain the highest count rate; and (3) use of two or more γ-ray sources surrounding the detector, in order to attain the geometrical and response advantages to be discussed in Sec. IV C.

We therefore constructed a PSM having the above-mentioned characteristics, to be employed for measurements *in vitro*.

B. Calibration of PSM device

The PSM was calibrated using K_2HPO_4–water solutions. The least-squares fit of calibration points (curve a in Fig. 6) gave the following results:

$$R = 0.0206 \text{ wt.\%} + 0.00224; \quad r = 0.999. \tag{9}$$

The measuring time was 10^3 s and the statistical error, $\Delta W = 5‰$ at $W = 30\%$.

It is to be noted that the statistical error that could be attained for measurements *in vivo* is expected to worsen a little due to absorption effects introduced by cortical bone and soft tissue.

C. Assessment of scattering volume

The scattering volume is defined as the intersection region between the two primary photon beams and the cone defined by the detector collimation (Fig. 7). The contribution to the detected spectrum from each point in SV can be calculated by considering the solid angles subtended by the sources and detector.

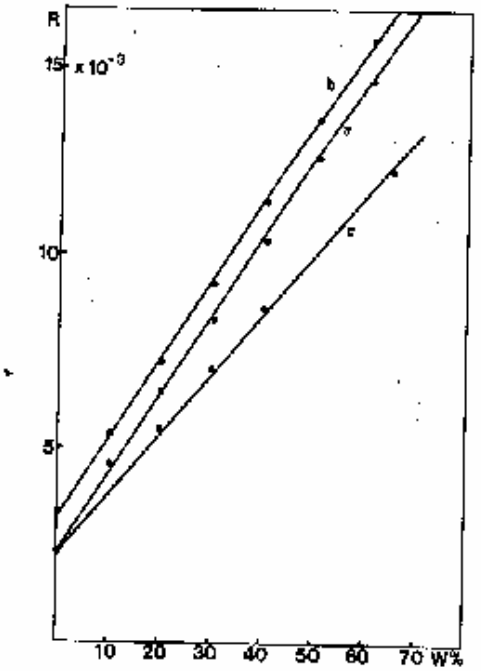

FIG. 6. Experimental R ratio vs K_2HPO_4 concentration in water solutions measured with PSM ($\vartheta = 135°$) in different experimental conditions. (a) K_2HPO_4 solutions placed inside SV (only self-absorption is considered); (b) R enhancement due to interposition of a Plexiglas sheet, 5 mm thick, between the detector and SV (both self-absorption and absorption are to be considered); (c) reduction of curve slope due to the presence of a 5-mm Plexiglas sheet inside the SV.

The idea of using two (or more) collimated sources (Fig. 7), placed around the detector, turns out to be very useful because the SV shape can be easily varied. In Figs. 8 and 9, the profiles, i.e., the scattered relative intensities due to a sample moving along the x and h axes, are reported for the two-sources measuring head.

The calculated profiles make it possible to evaluate the effective SV dimensions along principal axes by considering, for example, the one-tenth maximum value of profile curves. For our two-sources measuring system, these values correspond to lengths of 36 and 26 mm of h and x axes, respectively.

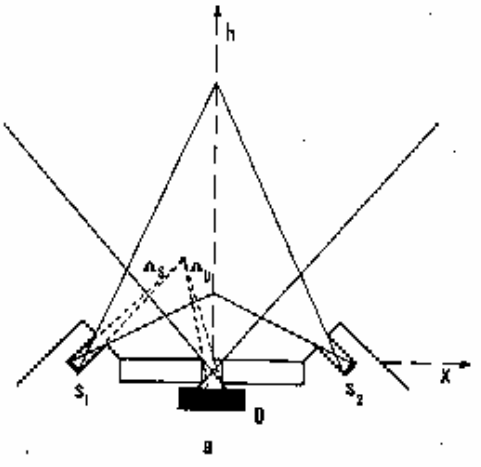

FIG. 7. Schematic drawing of the two-sources–detector geometry. Source (S_1, S_2) lead collimators: 10 mm deep, 3 mm wide. Detector (D) lead collimator: 7 mm deep, 6 mm wide.

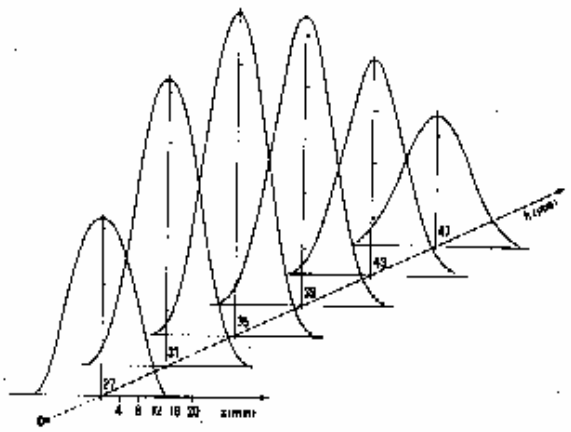

FIG. 8. The calculated scattered γ-ray relative intensity along the two principal axes x and h. These "profiles" allow one to estimate the scattering volume size (see text).

D. Statistical error and accuracy

Many factors could affect the precision and the accuracy of the coherent/Compton technique when applied to measurements *in vivo*, as pointed out by Ling *et al.*[3]

In the present work, statistical errors and correcting factors concerning the main sources of error have been theoretically and experimentally evaluated for phantoms only. The overall precision was not reported because it was not significant for our phantoms.

Correcting methods for absorption and self-absorption can be introduced for a backscattering geometry by using a simplified model in which reflecting layers (trabecular bone) and absorbing layers (soft tissue and cortical bone) are considered. Let us introduce thicknesses H_{st}, H_{cb}, and T, dealing with soft tissue, cortical bone, and trabecular bone, respectively. Then the G function in Eq. (2) can be written in the following approximated form (see Appendix):

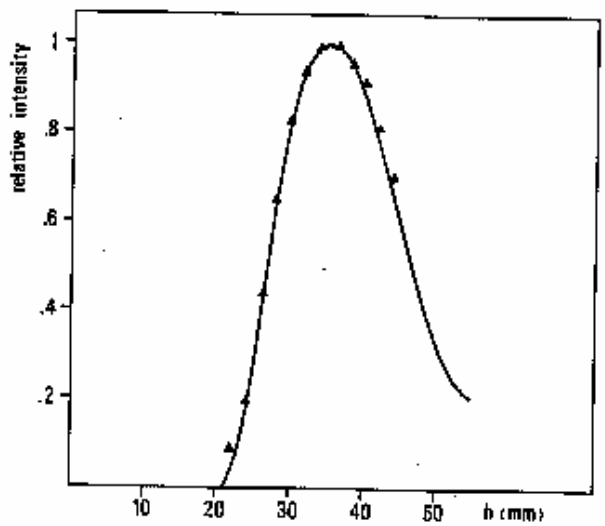

FIG. 9. Calculated profile along h axis. For comparison some experimental points, i.e., Compton-scattered relative intensities, are reported.

$$J_{st} = [\mu_{st}/\cos(\varphi) + \mu_{st}],$$

$$J'_{ch} = [\mu_{ch}/\cos(\varphi) + \mu'_{ch}],$$

$$J_{ch} = [\mu_{ch}/\cos(\varphi) + \mu_{ch}],$$

where μ_{th}, μ_{st}, and μ_{ch} are the linear attenuation coefficients at energy E_0; μ'_{th}, μ'_{st}, and μ'_{ch} are the linear attenuation coefficients at the Compton energy; ϵ_r and ϵ_c are the efficiencies at the above-mentioned energies; and $\varphi = 180° - \vartheta$.

The scattered intensities can then be written

$$I_c = I_0\, \epsilon_c\, d\, [\Sigma(\mu/d)_{C,i}\, W_i] \times \exp(J'_{st}\, H_{st} + J'_{ch}\, H_{ch}) \frac{[1 - \exp(-K'_{th}\, T)]}{K'_{th}}, \tag{A1}$$

$$I_r = I_0\, \epsilon_r\, d\, [\Sigma(\mu/d)_{R,i}\, W_i] \times \exp(J_{st}\, H_{st} + J_{ch}\, H_{ch}) \frac{[1 - \exp(-K_{th}\, T)]}{K_{th}}. \tag{A2}$$

The ratio between Eqs. (A2) and (A1) brings us to Eq. (2), where G is defined in Eq. (10), and

$$K_{st} = J'_{st} - J_{st}$$

and

$$K_{ch} = J'_{ch} - J_{ch}.$$

[1] P. Puumalainen, A. Uimarihuhta, E. M. Alhva, and H. Olkkonen, Radiology 120, 723 (1976).
[2] S. A. Kerr, K. Kouris, C. E. Webber, and T. J. Kennett, Phys. Med. Biol. 25, 1037 (1980).
[3] S. S. Ling, S. Rustgi, A. Karellas, J. D. Craven, J. S. Whiting, M. A. Greenfield, and R. Stern, Med. Phys. 9, 208 (1982).
[4] A. Karellas, I. Leichter, J. D. Craven, and M. A. Greenfield, Med. Phys. 10, 605 (1983).
[5] I. Leichter, A. Karellas, J. D. Craven, and M. A. Greenfield, Med. Phys. 11, 31 (1984).
[6] R. S. Holt, K. Kouris, M. J. Cooper, and D. F. Jackson, Phys. Med. Biol. 28, 1435 (1983).
[7] G. E. Gigante and S. Sciuti, Int. J. Appl. Radiat. Isot. 35, 481 (1984).
[8] J. H. Hubbell, W. J. Veigele, E. A. Briggs, R. T. Brown, D. T. Cromer, and R. T. Howerton, J. Phys. Chem. Ref. Data 4, 471 (1975); see also D. Schaupp, M. Schumacher, F. Smend, P. Rullhusen, and J. H. Hubbell, *ibid.* 12, 467 (1983).